

Article

Superparamagnetic Zinc Ferrite Nanoparticles as Visible-Light Active Photocatalyst for Efficient Degradation of Selected Textile Dye in Water

Rabid Ullah ¹, Fatima Khitab ^{1,2,*}, Hajera Gul ², Rozina Khattak ^{2,*}, Junaid Ihsan ³, Mansoor Khan ⁴, Abbas Khan ⁵, Zane Vincevica-Gaile ⁶ and Hani Amir Aouissi ^{7,8,9}

- ¹ Department of Chemistry, Sarhad University of Science and Information Technology, Peshawar 25000, Pakistan; rabidullahafri@gmail.com
- ² Department of Chemistry, Shaheed Benazir Bhutto Women University, Peshawar 25000, Pakistan; hajeragul11@yahoo.com
- ³ Department of Chemistry, Quaid-i-Azam University, Islamabad 45320, Pakistan; junaidihsan580@yahoo.com
- ⁴ Department of Chemistry, Kohat University of Science and Technology, Kohat 26000, Pakistan; mansoor009988@gmail.com
- ⁵ Department of Chemistry, Abdul Wali Khan University Mardan, Mardan 23200, Pakistan; abbas053@gmail.com
- ⁶ Department of Environmental Science, University of Latvia, LV-1004 Riga, Latvia; zane.gaile@lu.lv
- ⁷ Environmental Research Center (CRE), Annaba 23000, Algeria; aouissi.amir@gmail.com
- ⁸ LREAU Laboratory, Department of Geography and Spatial Planning, University of Sciences and Technology Houari Boumediene (USTHB), Algiers 16000, Algeria
- ⁹ Scientific and Technical Research Center on Arid Regions (CRSTRA), Biskra 07000, Algeria
- * Correspondence: fatima_khitab@yahoo.com (F.K.); rznkhattak@sbbwu.edu.pk or rznkhattak@yahoo.com (R.K.)



Citation: Ullah, R.; Khitab, F.; Gul, H.; Khattak, R.; Ihsan, J.; Khan, M.; Khan, A.; Vincevica-Gaile, Z.; Aouissi, H.A. Superparamagnetic Zinc Ferrite Nanoparticles as Visible-Light Active Photocatalyst for Efficient Degradation of Selected Textile Dye in Water. *Catalysts* **2023**, *13*, 1061. <https://doi.org/10.3390/catal13071061>

Academic Editor: Antonio Eduardo Palomares

Received: 29 April 2023
Revised: 23 June 2023
Accepted: 27 June 2023
Published: 30 June 2023



Copyright: © 2023 by the authors. Licensee MDPI, Basel, Switzerland. This article is an open access article distributed under the terms and conditions of the Creative Commons Attribution (CC BY) license (<https://creativecommons.org/licenses/by/4.0/>).

Abstract: Photocatalysis is a promising technology for the degradation of recalcitrant organic pollutants in water. In this study, superparamagnetic zinc ferrite nanoparticles (ZnFe_2O_4) were synthesized and characterized using scanning electron microscopy, X-ray diffraction, energy dispersive X-ray and Fourier transform infrared spectroscopy. The synthesized nanoparticles (NPs) of ZnFe_2O_4 were observed to have a photosensitive nature and showed characteristic visible-light-induced activation that was used for the photocatalytic degradation of a textile dye, Remazol brilliant violet 5R (RBV-5R). The effect of different operational parameters such as pH, H_2O_2 , catalyst dosage, concentration of RBV-5R and the reusability of ZnFe_2O_4 as well as scavengers were investigated under visible irradiation. The almost complete degradation (99.9%) of RBV-5R was observed at pH 10, 0.1 g of ZnFe_2O_4 and 6 mM of H_2O_2 in 30 min. The photocatalytic degradation of RBV-5R followed pseudo-first-order kinetics. The mineralization was calculated from total organic carbon (TOC) that was represented by 82% TOC removal in 30 min. The results revealed that visible-light-induced ZnFe_2O_4 photocatalysis may be a promising technology for the elimination of toxic organic dyes, such as RBV-5R, from water resources.

Keywords: visible light-assisted photocatalysis; zinc ferrite (ZnFe_2O_4) nanoparticles; Remazol brilliant violet 5R; water treatment; advanced oxidation processes

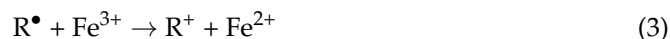
1. Introduction

Water is essential for life on Earth, but the tremendous problems it involves in terms of cleanliness, conservation, and shortage worry researchers [1]. Water scarcity is expected to be one of the biggest problems in the coming years. Water scarcity is a problem in many nations, and it becomes worse every year. One of the main causes of water pollution that leads to its scarcity is the industrial discharge of wastewater and effluents into pure water bodies. Since life is impossible without water, reusing water through wastewater treatment is one of the main goals in the fight to conquer and control the problems with water quality

and drinking water for human survival. The last few revolutionary decades in textile industries have resulted in the usage of tons of synthetic dyes [2]. According to estimates, the dye industries annually poison over 11 million tons of water, which accounts for close to 20% of all water pollution worldwide. Dyes are the most persistent contaminant in water because to their complex aromatic structure, resistance to degradation, high molecular weight, carcinogenic and mutagenic nature, propensity to screen sunlight, and stability [3]. The textile, paint, cotton, cosmetic, plastic, pharmaceutical, and food industries all use synthetic dyes in significant quantities. Untreated wastewater discharged into the nearby aquatic environment that contains dye presents a serious environmental risk. In addition to changing the color of water bodies, these dyeing effluents also release poisonous by-products that are harmful to many living things and can cause cancer and mutagenesis [4,5]. Sunlight cannot reach the aqueous system because of the cancer-causing pigments in water. The outcome is a slowdown in photosynthesis and harm to aquatic life [6]. Therefore, as a result of pollution brought on by industry, urbanization, and population growth, clean water is becoming scarce, and more and more expensive everywhere [7].

Numerous common procedures, such as coagulation, membranes, activated carbon, adsorption, sodium hypochlorite, filtration, microbial degradation, and electrochemical destruction, are used to remove undesired contaminants from wastewater [8–12]. The difficult formation of sludge, high chemical and operational expenses, and the propensity for pollutants to move from one step to another are among the primary downsides of each of these methods. Advanced oxidation techniques, particularly heterogeneous semiconductor-based photocatalysis, have emerged as highly promising and offer a significant potential for the degradation of numerous contaminants in wastewater over the past few decades [13–18]. Researchers used different photocatalysts such as Fe₂O₃ coated on TiO₂ [19], maghemite nanoparticles [20], phyco-synthesized ZnO [21], CeO₂/TiO₂/SiO₂ nanocatalysts, silver quantum dots immobilized on an exfoliated graphitic carbon nitride nanostructure [22], Ni-impregnated ZnO nanoparticles [23], Fe-doped titanic catalysts [24], Cu-ZnO [25], Ni-doped ZnO [26,27] and iodine-doped iron tungstate [28] for the degradation of various pollutants. The photocatalytic effectiveness of the catalysts for the degradation of pollutants under visible light is improved by the addition of various transition metals to produce composites based on binary and ternary metal oxides and heterojunctions [29]. Zinc ferrite nanoparticles are among them and are considered to be one of the most promising photocatalysts due to their fascinating physiochemical properties, better charge carrier separation features, and high efficiency for degradation in the visible light. When combined with hydrogen peroxide, zinc ferrite nanoparticles have a synergistic impact and produce a large number of free radicals that are necessary for the destruction of contaminants, i.e., RH (Equations (1)–(4)). The optical, structural, and photocatalytic properties of zinc ferrite nanoparticles are enhanced by the Zn ions. By acting as a charge trap, Fe³⁺ ions in zinc ferrite lower the rate of electron-hole recombination. The high activation efficiency and biocompatibility of Fe³⁺ ions provide the justification for its increased photocatalytic degradation impact on pollutants. Zinc ferrite functions as a potent photocatalyst due to the presence of Fe³⁺ ions and a narrow energy-band gap. It also has exceptional optical and magnetic properties. Its high surface area and small particle size contribute to its high reactivity. Consequently, several recent research initiatives have focused on the production of zinc ferrite. Several methods have been used for the synthesis of zinc ferrite, including hydrothermal [30] and solvothermal processes [31], sol-gel [32], co-precipitation [33] and combustion synthesis [34]. Due to its simple, quick synthesis reaction and inexpensive raw material, the combustion synthesis procedure was selected among the others for the production of zinc ferrite.





Zinc ferrite nanoparticles were selected for this study because of their higher potential to generate free radicals. After they were synthesized and characterized, it was found that they have a band gap in the visible region. In order to demonstrate their photocatalytic property, zinc ferrite nanoparticles' effect on the degradation of Remazol brilliant violet-5R was investigated. The azo dye Remazol brilliant violet-5R (RBV-5R), a member of the group of dyes used in the textile industry, was selected for photocatalytic degradation under visible light because it is extremely mutagenic, carcinogenic, hinders the growth of aquatic life, and is damaging to the environment [35,36]. The following factors were considered: pH, hydrogen peroxide, catalyst weight, and scavengers. Precise kinetic model representations were used to determine the degradation mechanism.

2. Results and Discussion

2.1. Characterization

SEM analysis was carried out to examine the morphology of the synthesized $ZnFe_2O_4$ sample. Figure 1 displays the SEM images at various magnifications. Three different types of surfaces, including granular or sphere-shaped, agglomerated, and a plan surface underlying the granular particles, have been observed in the sample. This could be as a result of ZnO, Fe_2O_3 , and $ZnFe_2O_4$ being present, respectively. As was already noted, during the combustion process, low-temperature combustion leads to the synthesis of pure zinc ferrite as well as some phases of ZnO and Fe_2O_3 [37]. Agglomeration might be a result of the existence of ferrite nanoparticles that group together because of their magnetic characteristics and high surface energies [38]. It is also possible that the radiation-based preparation of $ZnFe_2O_4$ contributed to the surface roughness and clusters of spherical nanoparticles [37,39].

The XRD analysis was also carried out for prepared $ZnFe_2O_4$. The Scherer equation was used to calculate the height, area of the peaks and their respective thicknesses. The peaks observed at a specific value of 2θ ranged from 24.3° to 77.88° . The height of the peaks was observed in the range of 4.08 to 87.36. The thickness of $ZnFe_2O_4$ nanoparticles was in the range of 1.8 to 9.3 nm, and, by applying Bragg's law, the value of 'd' was determined. The particle-to-particle distance ranged from 0.178 to 0.731 nm (Figure 2 and Table 1). The peaks at 35° , 37° , 42° , 53° , 57° , 62° , 70° , 72° and 74° values of 2θ corresponded to $ZnFe_2O_4$ while peaks at 33° , 48° , 68° and 69° corresponded to ZnO and peak at 35° and 54° values of 2θ are due to Fe_2O_3 . The $ZnFe_2O_4$ nanoparticles are according to the ICDD card no. 01-089-1012. ZnO and Fe_2O_3 are also present in the mixture. It was also reported by Oliveira et al. [40] that the combustion process at a low temperature results in the formation of pure zinc ferrite along with some phases of ZnO and Fe_2O_3 , which is also confirmed from XRD analysis of the synthesized zinc ferrite catalyst in this study.

Figure 3 represents the FTIR spectrum of $ZnFe_2O_4$ within the range from 500 to 4000 cm^{-1} . Vibrational bands are observed at approximately 3200 and 3500 cm^{-1} , which refer to the presence of adsorbed water molecules and the OH functional group [41]. Bands at 3900 and 1600 cm^{-1} refer to the H-O-H stretching vibration of adsorbed water molecules. Small peaks at 2900 and 1300 cm^{-1} may be assigned to the stretching vibration of the C-H bond. The peak near 1100 cm^{-1} corresponds to the CO_2 . The absorption peak present in the range of 600 to 1000 cm^{-1} refers to metal-oxygen ion vibrations located in the different phases. The small peak present in the range of 600 to 700 cm^{-1} attributes to the expansion of the Zn-O bond, and peak below 650 cm^{-1} may be assigned to the Fe-O intrinsic stretching vibration.

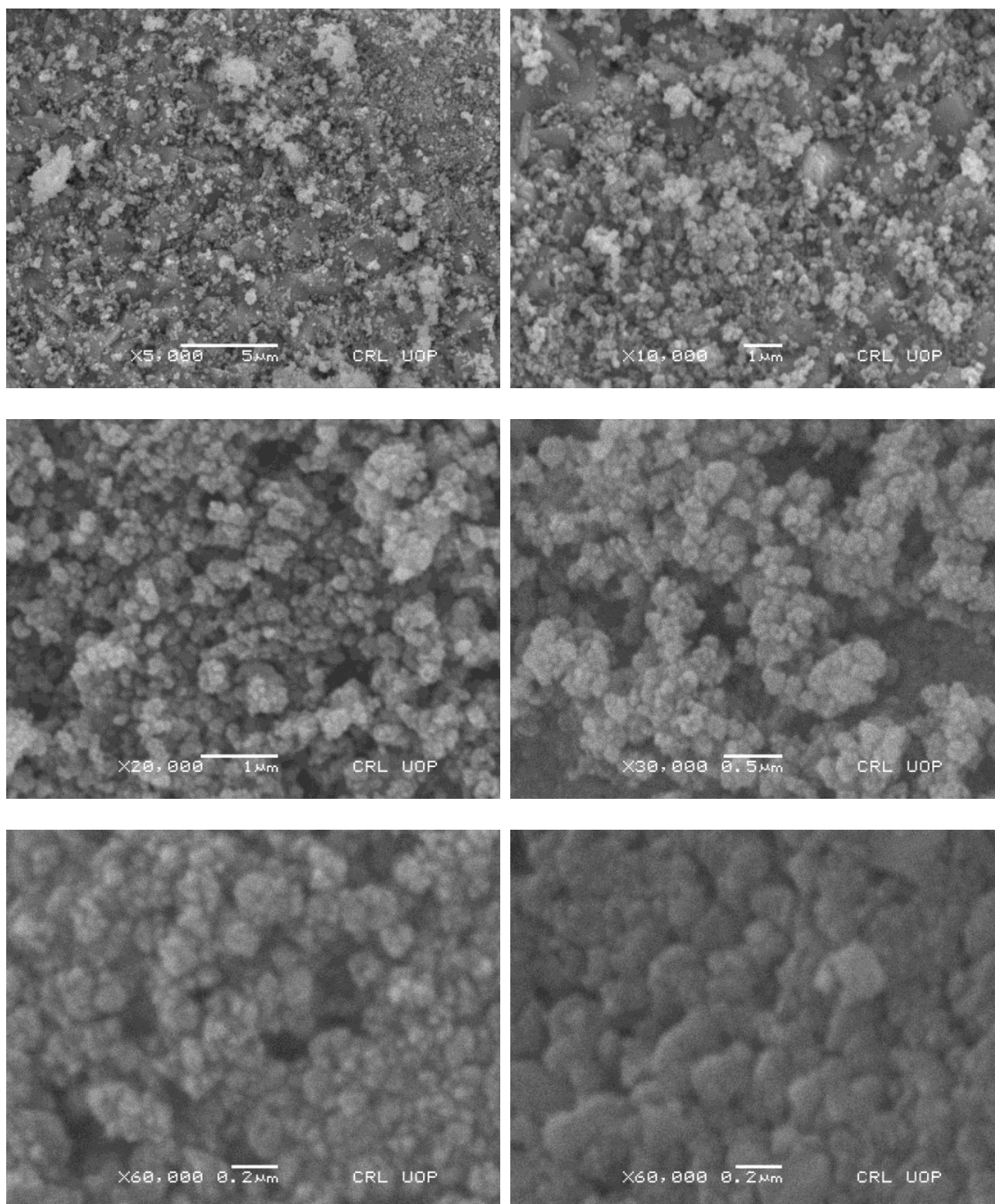


Figure 1. SEM images of ZnFe₂O₄ at different magnification.

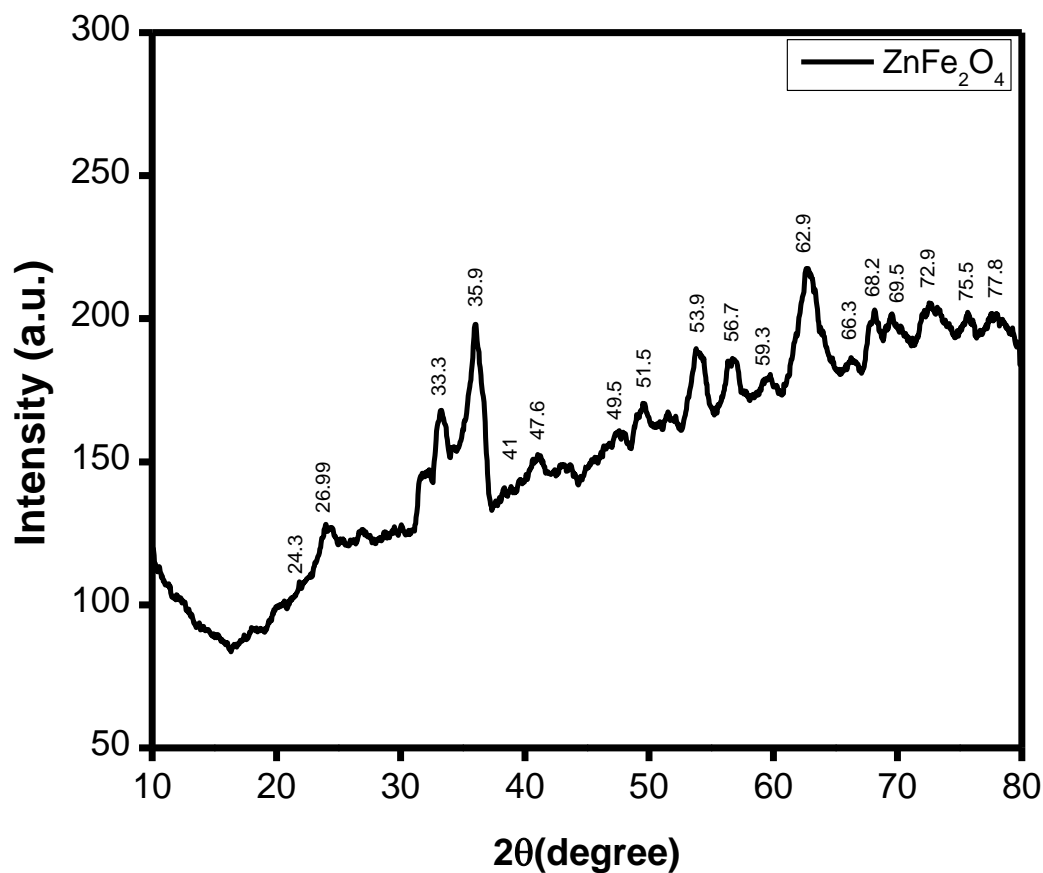


Figure 2. XRD pattern of the synthesized zinc ferrite powder.

Table 1. X-ray diffraction data for ZnFe_2O_4 .

2θ	Height from Base	Width (at Half Height)	Area	Thickness (nm)	d Bragg's Law
24.3	21.12	2.04923	45.76	3.916229	0.731977
26.99	4.08	0.8568	3.72	9.316631	0.660182
33.32	54.36	1.7135	99.16	4.589759	0.537373
35.95	87.36	2.1886	203.55	3.567794	0.49922
41.04	14.07	1.3422	9.85	5.728124	0.439501
47.65	38.223	3.56426	145.39	2.106921	0.38139
49.54	8.52	0.91466	8.29	8.149375	0.367706
51.57	7.22	0.84212	6.4759	8.777626	0.354165
53.99	30.34	1.55204	30.34	4.712999	0.339405
56.75	16.56	1.1772	20.75	6.135667	0.324173
59.61	6.65	1.1871	8.41	6.000593	0.309949
62.9	36.32	1.8565	71.79	3.772282	0.295273
66.35	3.99	0.83156	3.53	8.262954	0.281543
68.21	78.8	2.75204	273.21	2.469925	0.274758
69.54	5.68	0.62235	3.76	6.609569	0.178017
72.94	24.44	3.4749	90.4	1.899799	0.259185
75.65	6.71	0.79902	5.71	8.115423	0.251218
77.88	8.78	1.8761	17.55	3.403443	0.245121

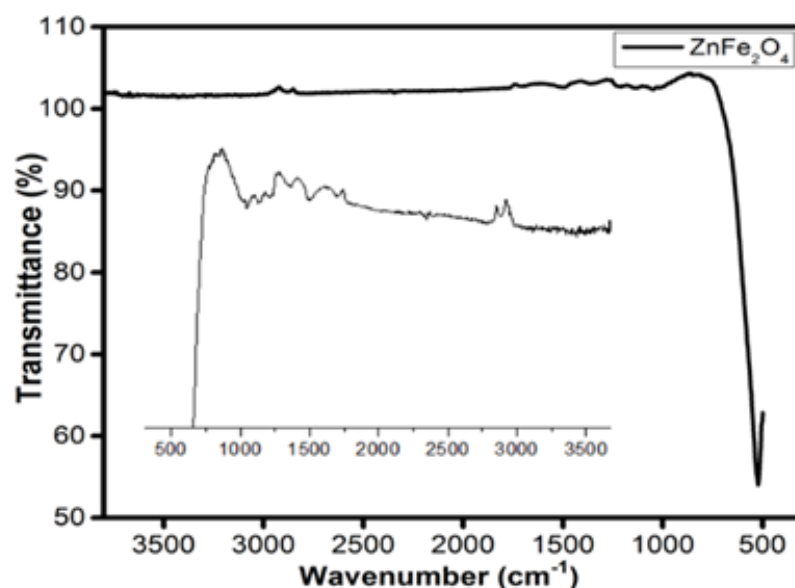


Figure 3. FTIR spectra of synthesized zinc ferrite catalyst.

An EDX study was carried out to determine the zinc ferrite's surface composition. ZnFe_2O_4 has been formed as evidenced by a peak of Zn, Fe, and O (Figure 4).

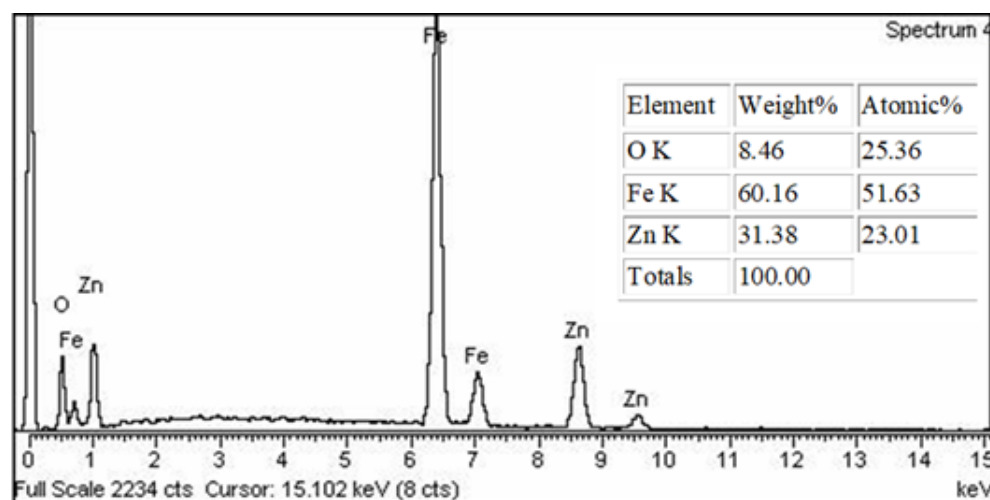
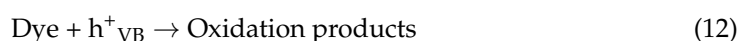
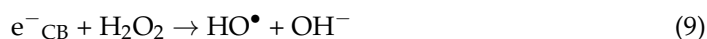
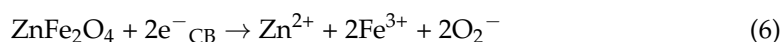
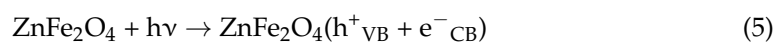


Figure 4. EDX spectrum of zinc ferrite catalyst.

2.2. Effect of Solution pHs

The degradation of RBV-5R was studied under acidic, neutral, and basic pH. The pH of the solution was varied from 2 to 10 using buffer as mentioned in materials and methods section. The percent degradation of RBV-5R as a function of pH is mentioned in Figure 5a. The pH study did not involve hydrogen peroxide. A 100 mg L^{-1} dye solution (50 mL), prepared in the selected buffer of known pH, was loaded with 0.1 g of the synthesized ZnFe_2O_4 and irradiated in the visible light as mentioned in the procedure in Section 3.4. It has been observed that both acidic and basic pH show high degradation of the dye as compared to neutral pH that was good over pH 4 where there is no significant degradation (Figure 5a,b). Equations (5)–(12) represent the reactions that may occur in the reaction vessel [42]. The maximum degradation of RBV-5R was 26.4% at pH 2 and it was 34% at pH 10. In acidic medium, the formation of hydroxyl radicals helps to the degradation of the dye according to Equations (5)–(9). According to Equation (9), the neutralization of the hydroxide ion causes the generation of the hydroxyl radical to be enhanced and expedited in extremely acidic media. However, it declines linearly even though pH 4

has the slowest rate of degradation and no discernible degradation of RBV-5R is seen after 60 min (Figure 5b). This might be as a result of the use of buffer solution, which contains different anions, as well as the positively charged surface of the catalyst, which might have prevented the dye from degrading by preventing the production of hydrogen peroxide, which would have produced a hydroxyl radical [43,44]. RBV-5R is an anionic dye, and as the pH rises above 4 up to the basic range, the protons produced in the reaction medium scavenge the production of hydroxyl ions, which speeds up the production of hydroxyl radical, and as a result the rapid degradation of the dye occurs in accordance with Equations (4) and (9)–(11) [45]. The linear correlation of the percent degradation of the dye as a function of pH is shown in Figure 5b. Furthermore, it was established that 6 was the point of zero charge. The ZnFe_2O_4 photocatalyst is supposed to have a positively charged surface at acidic pH levels, although a range of conjugate bases may diminish the catalyst's effectiveness in degrading RBV-5R. As a result, compared to non-buffer systems, the photocatalyst demonstrated a reduced performance in buffered solutions. This may also be supported by the buffer system's lower degradation percentage of the dye at pH 7 in comparison to that seen in the test in Section 3.4. Equation (10) may be the only source of hydroxyl production in the buffer system at pH 7, and it causes degradation at a lower rate and percentage in 60 min. The use of the synthesized photocatalyst might be helpful in industrial wastewater treatment because it performs well under acidic and basic conditions.



2.3. Effects of Catalyst Loading

The visible-light-induced catalytic degradation of RBV-5R was examined using different ZnFe_2O_4 dosages under optimum pH and oxidant condition. The catalyst dose was varied between 0.05 and 0.5 g, and the degradation was monitored for 30 min at pH 10, 6 mM H_2O_2 and 50 mL of 100 mg L^{-1} RBV-5R. It was determined that 30 min was the appropriate amount of time for degradation in the following study because no additional degradation was visible beyond 30 min up to 120 min. As the photocatalyst weight grew from 0.05 to 0.1 g, the degradation rate increased. At 0.1 g of ZnFe_2O_4 photocatalyst, RBV-5R shows the maximum degradation at a time interval of 30 min. The findings demonstrate that the degradation rate increased as the photocatalyst dose increased from 0.05 to 0.1 g, reaching its maximum producing 100% degradation in 30 min (Figure 6). The availability of more active sites on the catalyst surface and the penetration of visible light into the solution, which alter the light scattering and screening effect, are the reasons why the degradation rate accelerates with an increase in the catalyst load [46]. The overlap of the photocatalyst's surface and agglomeration may be the reason why a further increase (0.2 to 0.5 g) in catalyst dosage results in a decrease in the degradation rate (Figure 6). The high particle concentration in the reaction vessel may also contribute to decreased light penetration, which in turn affects photocatalysis efficiency.

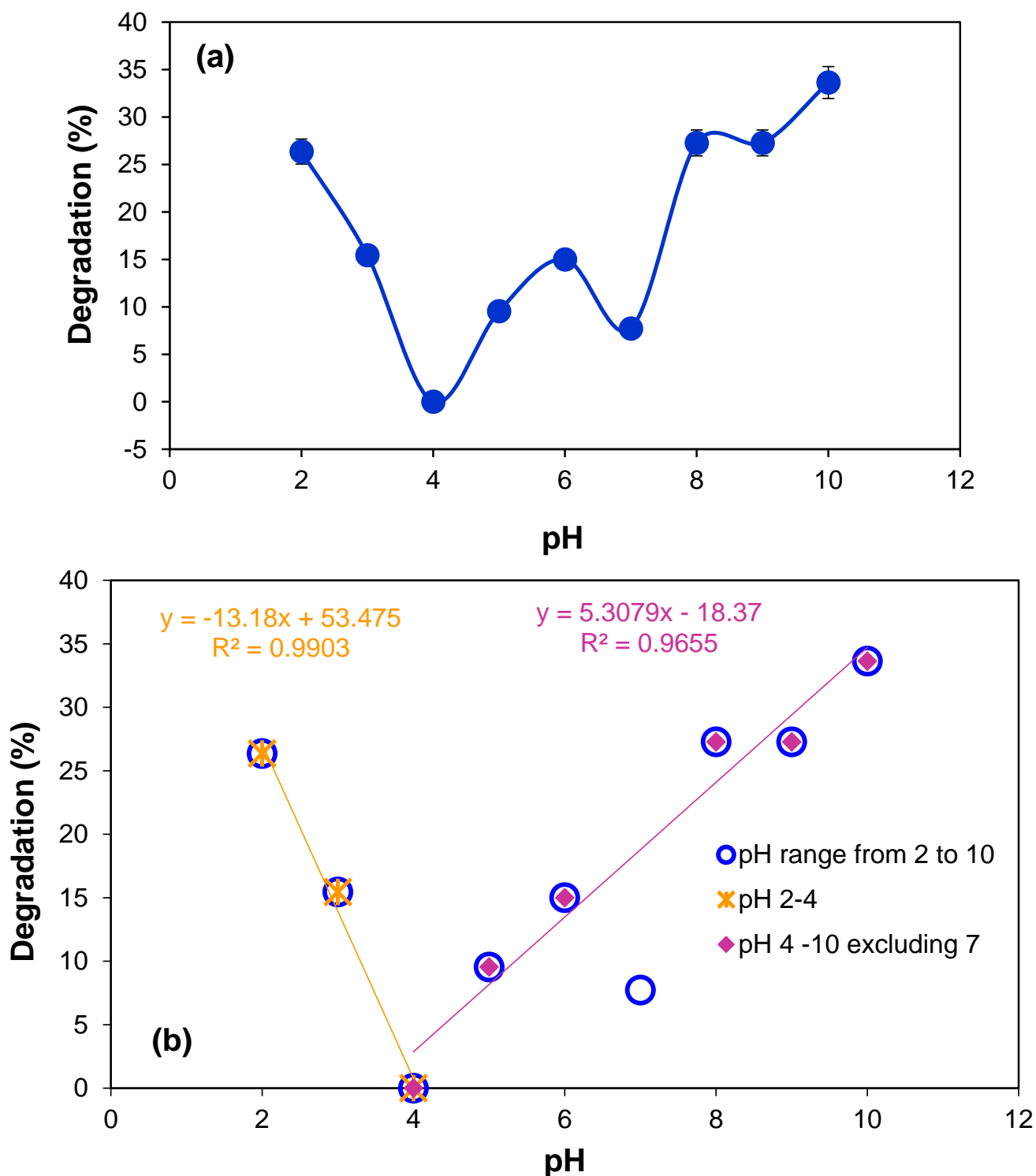


Figure 5. (a) Effect of pH on the photocatalytic degradation of RBV-5R at experimental conditions of 0.1 g ZnFe₂O₄ photocatalyst with 100 mg L⁻¹ initial concentration of RBV-5R. (b) pH dependence of the degradation of RBV-5R.

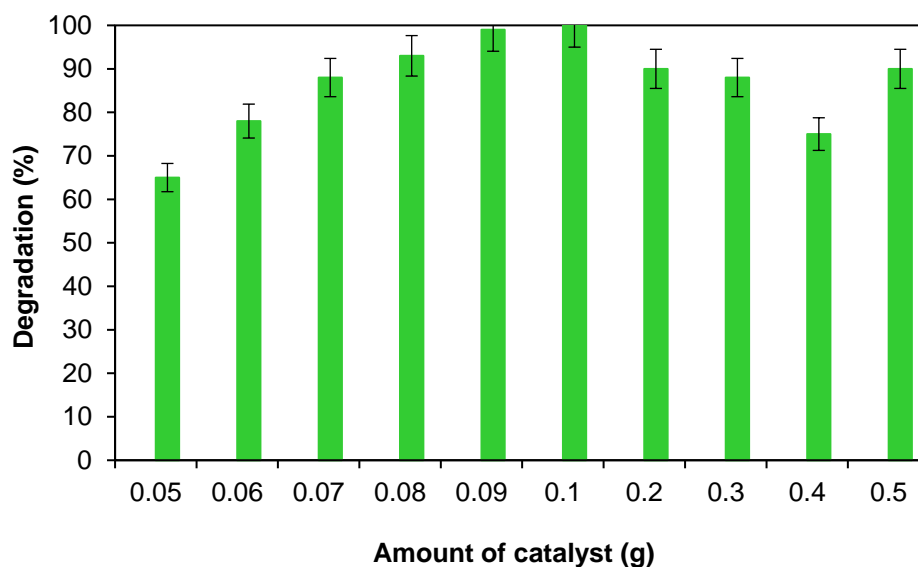
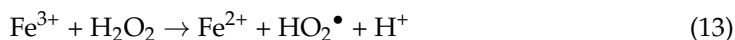


Figure 6. Effect of catalyst loading on the photocatalytic degradation of 100 mg L^{-1} (50 mL) RBV-5R at pH 10 in the presence of $6 \text{ mM H}_2\text{O}_2$ in 30 min.

2.4. Effects of the Concentration of H_2O_2

The effect of H_2O_2 on the degradation of 100 mg L^{-1} (50 mL) RBV-5R was examined at an optimum pH of 10, 0.1 g of ZnFe_2O_4 , and 30 min. The initial H_2O_2 concentration was varied from 2 to 10 mM. At $6 \text{ mM H}_2\text{O}_2$, the RBV-5R showed a 99% degradation (Figure 7). The addition of H_2O_2 increased the concentration of hydroxyl radicals, which caused the highest degradation [46]. However, the effectiveness of dye degradation showed no discernible results at higher H_2O_2 concentrations. This is due to the fact that, as Equations (13)–(18) demonstrate, hydroxyl radicals recombine and are scavenged [47]. The TOC analysis was also performed, and was found to be 82% after the degradation of the dye.



2.5. Effect of Initial Dye Concentration

The influence of initial dye concentration on the percent degradation of RBV-5R was investigated using 20, 40, 60, 80, and 100 mg L^{-1} of the dye. At room temperature, 0.1 g of ZnFe_2O_4 photocatalyst was added to the reaction mixture containing $6 \text{ mM H}_2\text{O}_2$ and pH 10. Figure 8 shows that the dye's degradation was inversely related to its initial concentration. At 100 mg L^{-1} of RBV-5R, there was a prominent reduction in the percent degradation as the degradation rate decreased with increasing initial dye concentration (Figure 8). A higher initial concentration of RBV-5R leads to a lower rate of degradation since the catalyst absorbs less light due to its low absorption rate. In larger concentrations, the dye absorbs light more thoroughly. The catalyst's ability to be illuminated as a result is harmed, which lowers the yield of free radicals [46].

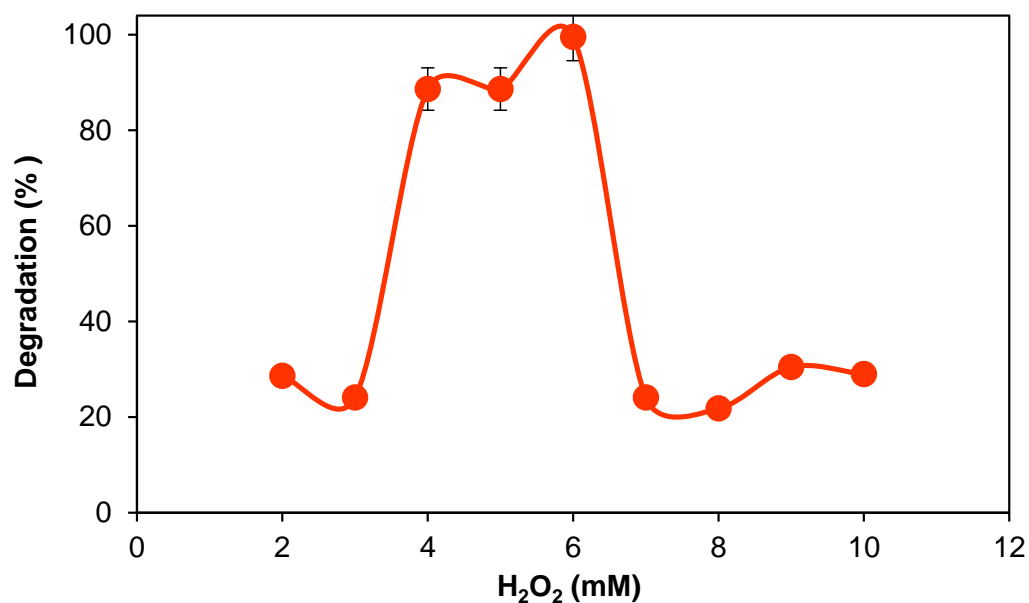


Figure 7. Effect of oxidant (H_2O_2) concentration on the photocatalytic degradation of 100 mg L^{-1} RBV-5R at pH 10 loaded with $0.1 \text{ g ZnFe}_2\text{O}_4$.

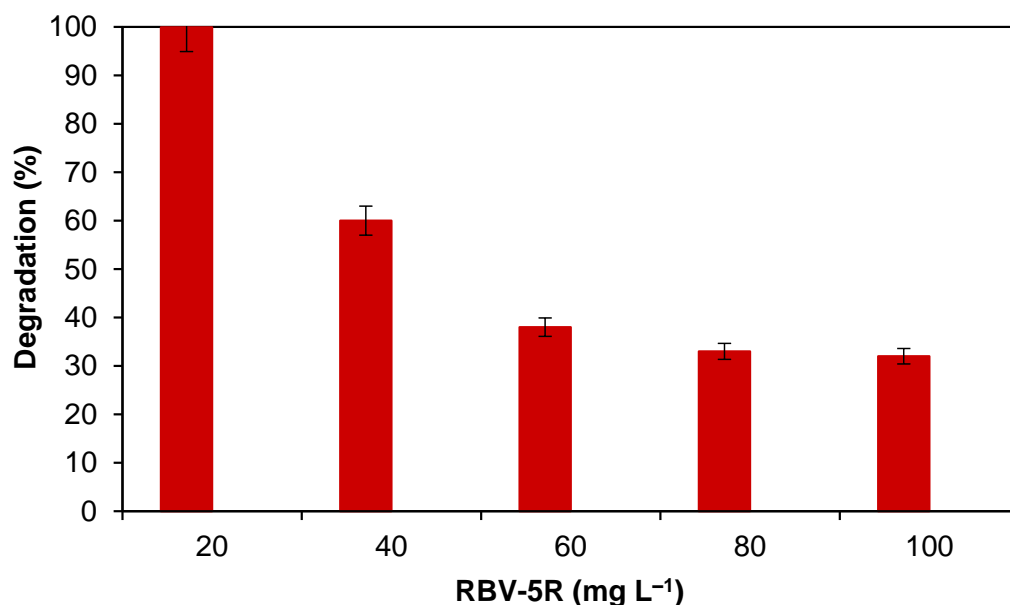


Figure 8. Effect of initial dye concentration on the photocatalytic degradation of RBV-5R at $0.1 \text{ g ZnFe}_2\text{O}_4$, pH 10, $6 \text{ mM H}_2\text{O}_2$ and 30 min time frame.

2.6. Catalyst Reusability

To study the effectiveness and stability of the ZnFe_2O_4 photocatalyst, reusability analysis was carried out under optimized conditions. After each successive run, the ZnFe_2O_4 photocatalyst was filtered and washed with distilled water and organic solvents (methanol and ethanol) three times. The dried photocatalyst was collected, reweighed and reused for the second time using optimized conditions of pH and H_2O_2 and 100 ppm of RBV-5R. The catalyst's reusability was checked for three runs. The degradation for the RBV-5R in the reusability test was 99, 98 and 97%, respectively (Figure 9a,b). The decrease in the degradation may be due to weight loss in the filtration and washing of the catalyst. As illustrated in Figure 9a, the degradation process for each run is distinct as a function of time. When comparing maximum degradation over a shorter time, third usage exceeds second use, which outperforms first use. This can be as a result of surface modifications

that take place after each run. The kinetic order of RBV-5R degradation after each run, however, is different as seen in Figure 9c–e. This could be the case since the catalyst surface may function differently but still effectively following thorough washing for reusability. This results in the first run showing a first order (Figure 9c), the second run showing a third order (Figure 9d), and the third run showing a zero order (Figure 9e).

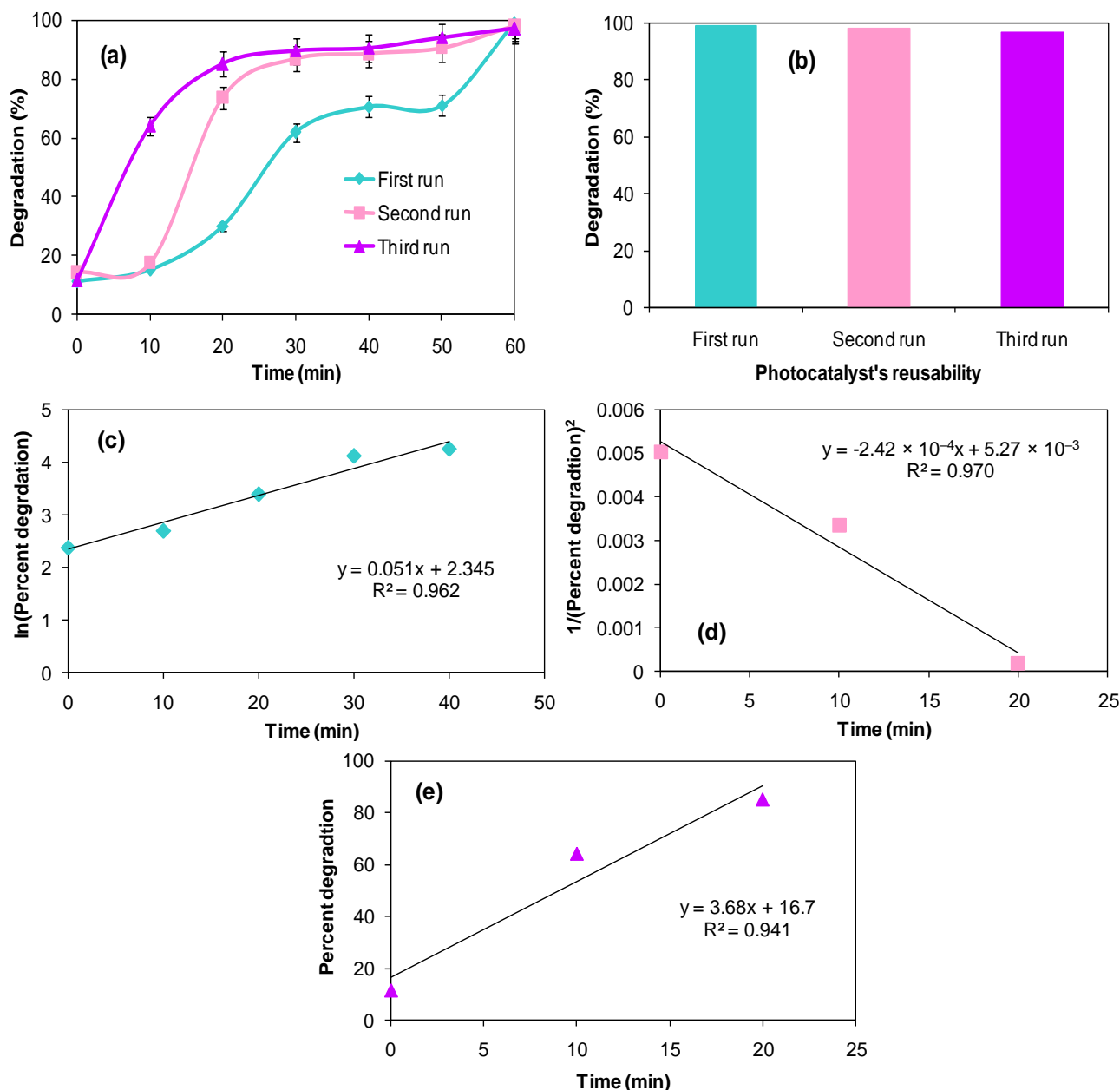


Figure 9. Catalyst reusability runs for the degradation of RBV-5R dye. (a) Percent degradation of RBV-5R as a function of time. (b) Plot of ZnFe₂O₄ photocatalyst's reusability for three runs. (c) Plot of first order kinetics for first run. (d) Plot that shows third order kinetics for second reusability run. (e) Plot that indicates zero-order kinetics for third run.

After each successive run, the leaching of Fe was also checked using AAS (atomic absorption spectroscopy), and it was found to be very negligible, i.e., 0.28 mg L⁻¹, which was lower than the permissible limit of European Union directives, i.e., 2.0 mg L⁻¹. Considering the commercial applications of the synthesized ZnFe₂O₄ photocatalyst, the effect of catalyst settling time was also investigated and was found to be 2 min for 5 g of photocatalyst for settling down.

While keeping in mind how the suggested approach will be used on commercial samples, the impacts of scavengers were also examined. Scavengers were administered at different concentrations, such as 0.05, 0.1 and 0.15 mM, and the percentage of degradation was calculated. NaCl shows a small reduction in degradation when compared to MgCl₂ (Figure 10). These anions slow down the rate of degradation, maybe as a result of their interactions with the photocatalyst's surface, which simultaneously inhibits the generation of free radicals [40] (Oliveira et al., 2020). Magnesium chloride inhibits photocatalytic degradation more than sodium chloride does because it contains two anions.

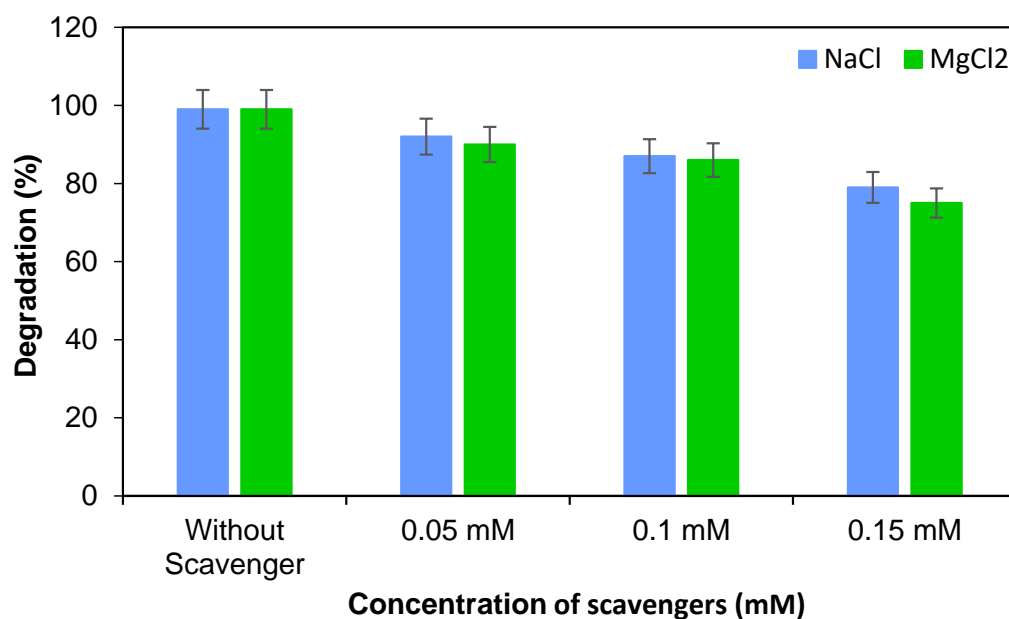


Figure 10. Effect of scavengers on the photocatalytic degradation of RBV-5R by ZnFe₂O₄.

2.7. Kinetic Models

The order of reaction was determined by implementing the pseudo-first-order (PFO) and pseudo-second-order (PSO) kinetic models (Figure 11a,b). The following (Equations (19) and (20)) represent the linear form of the PFO and PSO kinetic models, respectively, with the R² value for PFO = 0.961 indicating that degradation of RBV-5R followed pseudo-first-order kinetics. The results further reveal that the rate of visible-light-induced degradation using the ZnFe₂O₄ photocatalyst is dependent on the concentration of RBV-5R as other parameters were in excess [48]. The observed pseudo-first-order rate constant (k_{obs}) was determined to be 0.23 min⁻¹.

$$\ln C_t = \ln C_i - k_{obs}t \quad (19)$$

$$\frac{1}{C_t} = \frac{1}{C_i} + k_{obs}t \quad (20)$$

2.8. Photocatalytic Degradation Mechanism of RBV-5R and Comparison with Other Methods

When ZnFe₂O₄ is illuminated to the visible light under optimized conditions, the electrons present in the valence band jump to the conduction band, leaving holes behind in the valence band. In this way, an electron-hole pair is generated, and this generated e⁻/h⁺ pair reacts with water molecules and atmospheric oxygen to produce free radicals. The free hydroxyl radicals and hydrogen peroxide react with Fe(III) present in the photocatalyst ZnFe₂O₄, and subsequently initiate a Fenton-like reaction. Those free radicals are highly reactive species that react with the dye molecules and derivatives of RBV-5R. The generation of Fe(II) on the surface of the photocatalyst speeds up the degradation by producing more radicals. During the degradation process, many unstable intermediates such as 2-amino-5-dimethylamino-benzene sulfonic acid anion, dimethyl-(4-nitro-phenyl)-amine, 4-amino-

benzenesulfonic acid and 4-nitro-benzenesulfonic acid are formed [49], which are attacked by free radicals, and the degradation products are usually CO_2 , H_2O and mineral acids (Figure 12). The plausible degradation mechanism is given in Figure 13. The proposed degradation method was compared with other methods using different photocatalysts, and the comparative analysis is shown in Table 2. The proposed work was found to be more effective.

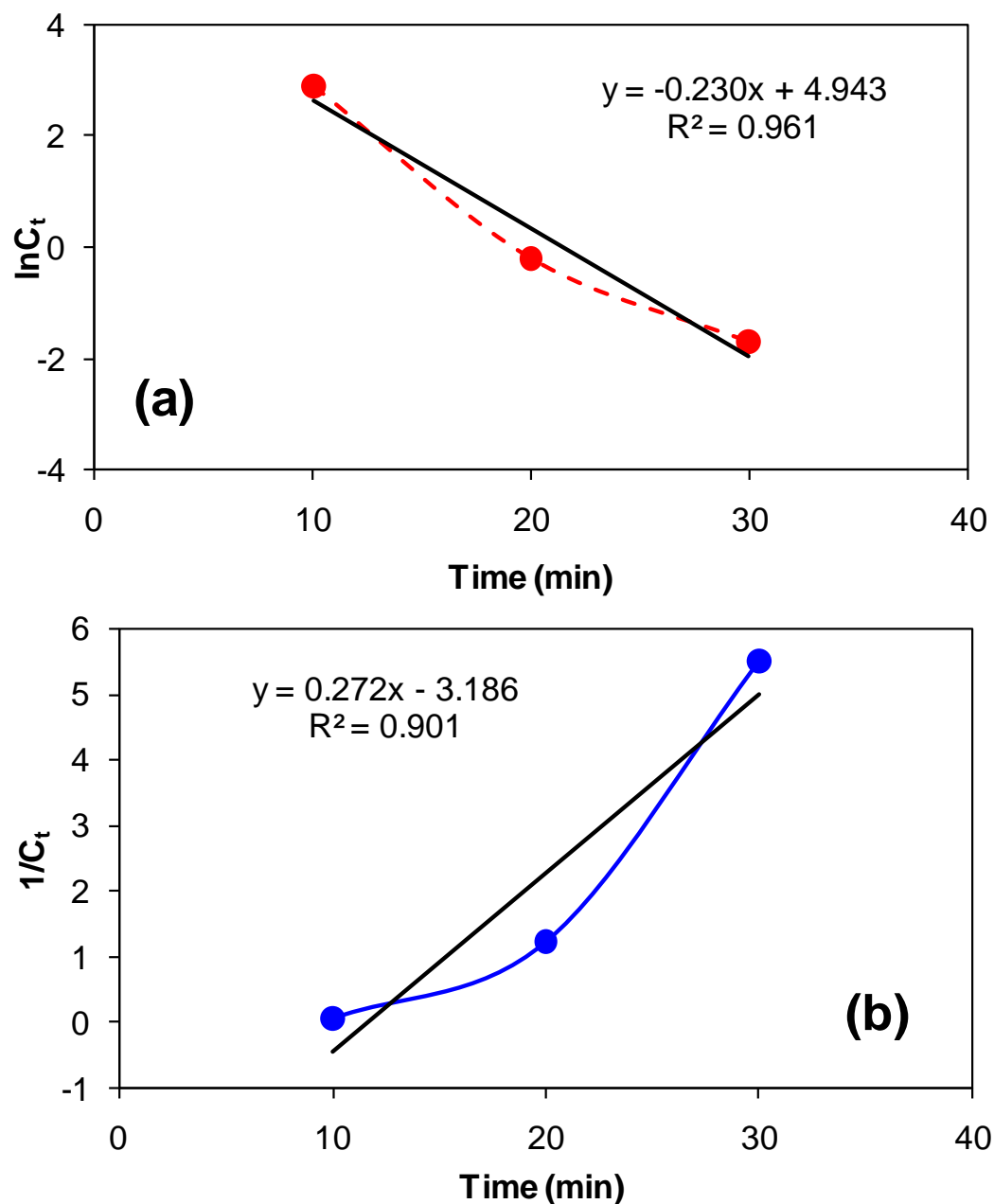


Figure 11. Pseudo-first-order (a) and pseudo-second-order (b) kinetic models for RBV-5R degradation by ZnFe_2O_4 .

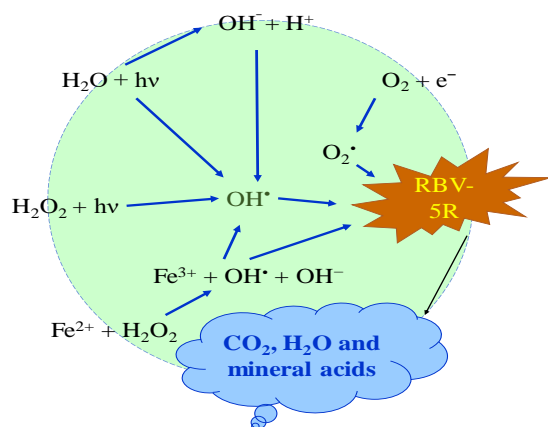


Figure 12. Reactions occurring during the photocatalytic degradation of RBV-5R.

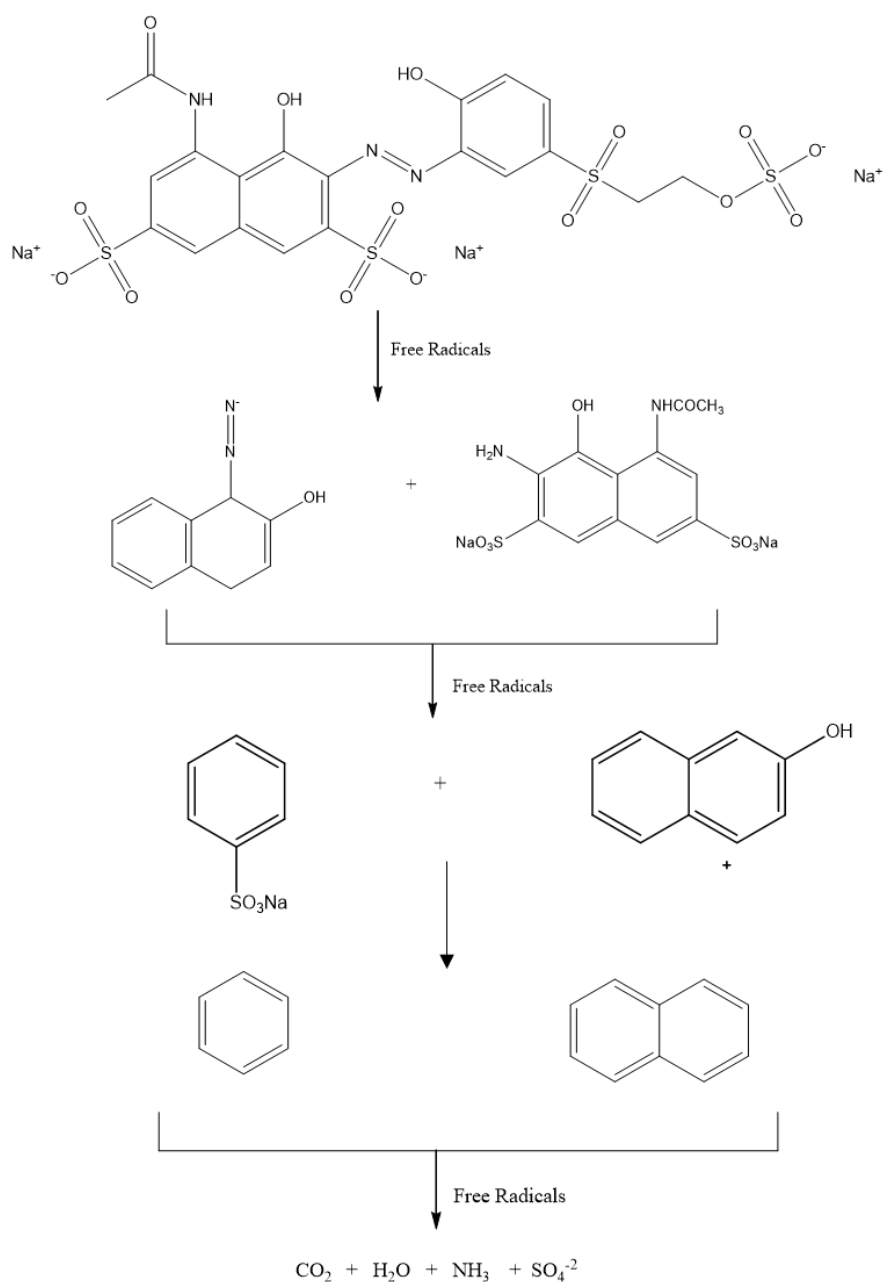


Figure 13. Plausible degradation mechanism of RBV-5R.

Table 2. Comparison of the proposed method with other methods used for the degradation of RBV-5R.

Method	Source of EMR	Catalyst	Time	% Degradation	References
Biological degradation	Trichoderma species	Trichoderma koningiopsis	12 days	73%	[50]
Biological degradation	Bacteria	Potential bacterial strain GSM	38 h	70%	[51]
Photocatalysis	Blue light-emitting diode (LED)	Fe-doped titania	120 min	100%	[24]
Photocatalysis	UV lamp	Zinc oxide	90 min	100%	[52]
Photocatalytic	100 W tungsten lamp	Zinc ferrite	30 min	99%	Present work

3. Materials and Methods

3.1. Materials

All the used reagents were of analytical grade. Without additional purification, the reagents $\text{Zn}(\text{NO}_3)_2 \cdot 6\text{H}_2\text{O}$ (zinc nitrate hexahydrate), $\text{Fe}(\text{NO}_3)_3 \cdot 9\text{H}_2\text{O}$ (iron nitrate nonahydrate), and $\text{CO}(\text{NH}_2)_2$ (urea) (99.5%, Synth) were purchased from Sigma-Aldrich and used directly in the synthesis. RBV-5R was imported from Boss Chemical Industry Co., Ltd., Jinan, China. Britton–Robinson buffer of Darmstadt was used to adjust pH. All the experiments were performed in triplicate and the results are the average of those trials.

3.2. Instruments

The absorbance measurements were carried out by the Double-Beam Hitachi U-2900/U-2910 model UV/Visible Spectrophotometer by using matched 1 cm quartz cells and at a maximum wavelength of RBV-5R (560 nm). A tungsten filament lamp of 100 W was used as a source of visible light for the photocatalytic degradation of RBV-5R.

The surface morphology of ZnFe_2O_4 was analyzed by a JSM5910 (JEOL, Tokyo, Japan) scanning electron microscope (SEM). The samples were coated using a thin layer of aluminum stub for SEM analysis using double-adhesive carbon tape. For the determination of total organic compounds (TOC), the TOC-VCPH analyzer (Shimadzu Co., Nagoya, Japan) was used for the measurement. For stirring, the XMTD-702 model magnetic stirrer was used. The XRD pattern for the sample was analyzed using an X-ray diffractometer (DRON-8). FTIR analysis was performed on a Shimadzu IRTracer-100. A pH meter (Model-Hanna Edge. III. 2020) was used for pH measurements.

3.3. Synthesis of Superparamagnetic Zinc Ferrite Nanoparticles

Visible-light-induced superparamagnetic zinc ferrite nanoparticles were prepared using a combustion process in a solution [53]. A weight of 12.31 g of zinc nitrate hexahydrate, 33.44 g of iron nitrate nonahydrate and 15.57 g of $\text{CO}(\text{NH}_2)_2$ (as fuel) were used in the solution combustion process to produce ZnFe_2O_4 . The molar ratio of Zn and Fe in the synthesis of zinc ferrite nanoparticles is 1:2 [40]. At 70 °C, the reagents were mixed in 40 mL of distilled water and stirred to mix them thoroughly. The solution was then placed in a muffle furnace and heated to 500 °C for 10 min. The precipitates were powdered and calcined in a furnace at a temperature of 500 °C for two h. The prepared ZnFe_2O_4 nanoparticles were first characterized and then used as a visible light-induced photocatalyst to degrade the selected dye.

3.4. Photocatalytic Study

Starting with a test for potential adsorption–desorption, 0.1 g of zinc ferrite was added to the solution of RBV-5R, 100 ppm/100 mL, and the mixture was stirred in the dark for 30 min. The dye's absorbance was ineffectively changed in 30 min, indicating that adsorption–desorption is ineffective in this situation. To determine how well ZnFe_2O_4 works as a photocatalyst, a preliminary test was carried out. For this reason, three tests

totaling 60 min each were carried out in the dark, under UV light, and under visible light. For the photocatalytic test, a known amount, 0.1 g of ZnFe_2O_4 sample, was added to 100 mL of RBV-5R solution with the selected initial concentration, i.e., 100 ppm (mg L^{-1}). RBV-5R was removed by 8% in the dark in 60 min, but it was removed by 19% in the same amount of time when exposed to UV light. This difference may be caused by RBV-5R's adsorption on the photocatalyst surface in the dark and zinc ferrite's poor photosensitivity when exposed to UV light, respectively. The degradation rose to 26% in 60 min when the solution was exposed to visible light, proving that ZnFe_2O_4 is a visible light-induced photocatalytic material [40]. As a result, the catalytic effect of ZnFe_2O_4 was studied under visible light irradiation by a 100 W lamp for the degradation of RBV-5R textile dye in an aqueous solution for 60 min. RBV-5R textile dye was selected as a pollutant.

For a typical photocatalytic test, a known amount, 0.1 g of ZnFe_2O_4 sample was added to 50 mL of RBV-5R solution with the selected initial concentration, i.e., 100 ppm (mg L^{-1}) and then exposed to visible light. The pH of the solution was adjusted by Britton–Robinson buffer in the range of pH 2 to 10 for revealing the pH effect. In the subsequent experiments, a 50 mL solution of RBV-5R (selected concentration) was loaded with zinc ferrite at the optimal pH, catalyst dose, and oxidizing agent. This solution was then exposed to visible light to check for degradation. Every 10 min, a 5 mL aliquot was taken and diluted to a volume of 25 mL. The degree of decolorization of the RBV-5R dye solution was assessed by measuring the absorbance at the maximum wavelength with a UV/Vis spectrophotometer. Equation (21) was used to calculate the % degradation of RBV-5R, and Equation (22) was used to calculate the contents of total organic compounds (TOC) in the selected samples before and after photocatalytic degradation [43].

$$\% \text{Degradation} = \frac{C_i - C_f}{C_i} \times 100 \quad (21)$$

$$\text{TOC} = \frac{\text{TOCC}_0 - \text{TOCC}_f}{\text{TOCC}_0} \times 100 \quad (22)$$

where, C_i and TOCC_0 are the initial concentrations, and C_f and TOCC_f represent the final concentrations in mg L^{-1} of dye after irradiation. Optimum conditions for the photocatalytic degradation of RBV-5R were determined by studying various factors such as pH, oxidant, catalyst dose, the dye's initial concentration and the catalyst's reusability. All the experiments were performed at room temperature, i.e., 27 ± 2 °C [40].

4. Conclusions

In this study, visible-light-activated superparamagnetic zinc ferrite nanoparticles (ZnFe_2O_4) were synthesized by a simple combustion process and were tested for the degradation of a model organic dye, i.e., Remazol brilliant violet 5R (RBV-5R) in water. The degradation of RBV-5R was higher under acidic and basic conditions while lower at a neutral pH in buffer system. The visible-light-activated ZnFe_2O_4 photocatalysis resulted in 100% degradation of RBV-5R and 82% total organic carbon removal in 30 min in the presence of hydrogen peroxide. The synthesized photocatalyst showed good reusability efficiency for three consecutive runs such as 99, 98 and 97%, respectively. The kinetic study revealed that the degradation of RBV-5R in water by ZnFe_2O_4 photocatalysis followed pseudo-first-order kinetics. From the results, it was concluded that visible-light-induced ZnFe_2O_4 photocatalysis was a promising technology for eliminating toxic organic dyes, such as RBV-5R, from the water environment.

Author Contributions: Conceptualization, F.K. and R.K.; data curation, R.K., A.K., Z.V.-G. and H.A.A.; formal analysis, H.G., R.K. and A.K.; funding acquisition, R.K.; investigation, R.U., F.K. and R.K.; methodology, R.U., F.K. and H.G.; resources, F.K., R.K. and H.A.A.; software, J.I. and M.K.; supervision, F.K.; validation, R.K., J.I., M.K. Z.V.-G. and H.A.A.; visualization, F.K. and R.K.; writing—original draft, R.U. and F.K.; writing—review and editing, R.K., Z.V.-G. and H.A.A. All authors have read and agreed to the published version of the manuscript.

Funding: This research received no external funding.

Data Availability Statement: Not applicable.

Acknowledgments: Fatima Khitab and Rozina Khattak acknowledge the technical support of the Shaheed Benazir Bhutto Women University, Peshawar, Pakistan.

Conflicts of Interest: The authors have no conflict of interest.

References

1. Raimi, M.O.; Ayibatobira, A.A.; Anu, B.; Odipe, O.E.; Deinkuro, N.S. 'Digging deeper' evidence on water crisis and its solution in Nigeria for Bayelsa state: A study of current scenario. *Int. J. Hydrol.* **2019**, *3*, 244–257.
2. Sanakousar, F.; Vidyasagar, C.; Jiménez-Pérez, V.; Prakash, K. Recent progress on visible-light-driven metal and non-metal doped ZnO nanostructures for photocatalytic degradation of organic pollutants. *Mater. Sci. Semicond. Process.* **2022**, *140*, 106390. [[CrossRef](#)]
3. Panchal, D.; Sharma, A.; Pal, S. Novel photocatalytic techniques for organic dye degradation in water. In *Photocatalytic Degradation of Dyes*; Elsevier: Amsterdam, The Netherlands, 2021; pp. 1–22.
4. Rajendran, R.; Kiruthika, S.; Saranya, P.; Mohan, A.; Vaishali, C. Biodecolorization of Azo Dye Mixture (Remazol Brilliant Violet 5R and Reactive Red 120) by Indigenous Bacterial Consortium Obtained from Dye Contaminated Soil. *Malays. J. Microbiol.* **2021**, *18*, 68–78.
5. Sultana, S.; Rehan, K.; Rehan, I.; Ali, F.; Waris, S.; Zahoor, M.; Salman, S.M.; Khan, S.; Rehan, M.S. Physicochemical and instrumental characterization of rice husk and its potential use as a low cost adsorbent for mutagenic dye bromophenol blue. *Z. Phys. Chem.* **2021**, *235*, 1263–1277. [[CrossRef](#)]
6. Bano, K.; Mittal, S.K.; Singh, P.P.; Kaushal, S. Sunlight driven photocatalytic degradation of organic pollutants using a MnV₂O₆/BiVO₄ heterojunction: Mechanistic perception and degradation pathways. *Nanoscale Adv.* **2021**, *3*, 6446–6458. [[CrossRef](#)]
7. Sarkar, S.; Ponce, N.T.; Banerjee, A.; Bandopadhyay, R.; Rajendran, S.; Lichtfouse, E. Green polymeric nanomaterials for the photocatalytic degradation of dyes: A review. *Environ. Chem. Lett.* **2020**, *18*, 1569–1580. [[CrossRef](#)]
8. Gidstedt, S.; Betsholtz, A.; Falås, P.; Cimbritz, M.; Davidsson, Å.; Micolucci, F.; Svahn, O. A comparison of adsorption of organic micropollutants onto activated carbon following chemically enhanced primary treatment with microsieving, direct membrane filtration and tertiary treatment of municipal wastewater. *Sci. Total Environ.* **2022**, *811*, 152225. [[CrossRef](#)]
9. Gul, S.; Kanwal, M.; Qazi, R.A.; Gul, H.; Khattak, R.; Khan, M.S.; Khitab, F.; Krauklis, A.E. Efficient removal of methyl red dye by using bark of hopbush. *Water* **2022**, *14*, 2831. [[CrossRef](#)]
10. Greaves, J.; Fischer, R.J.; Shaffer, M.; Bivins, A.; Holbrook, M.G.; Munster, V.J.; Bibby, K. Sodium hypochlorite disinfection of SARS-CoV-2 spiked in water and municipal wastewater. *Sci. Total Environ.* **2022**, *807*, 150766. [[CrossRef](#)]
11. El Bouraie, M.; El Din, W.S. Biodegradation of Reactive Black 5 by *Aeromonas hydrophila* strain isolated from dye-contaminated textile wastewater. *Sustain. Environ. Res.* **2016**, *26*, 209–216. [[CrossRef](#)]
12. Nippatlapalli, N.; Selvaraj, A. A study on the removal of long chain perfluorodecanoic acid in simulated aqueous solution using enhanced electrochemical technique: Metabolites, kinetic and isotherm model analysis. *J. Water Process Eng.* **2022**, *49*, 103045. [[CrossRef](#)]
13. Park, Y.; Kim, S.; Kim, J.; Khan, S.; Han, C. UV/TiO₂ photocatalysis as an efficient livestock wastewater quaternary treatment for antibiotics removal. *Water* **2022**, *14*, 958. [[CrossRef](#)]
14. Ara, A.; Khattak, R.; Khan, M.S.; Begum, B.; Khan, S.; Han, C. Synthesis, characterization, and solar photo-activation of chitosan-modified nickel magnetite bio-composite for degradation of recalcitrant organic pollutants in water. *Catalysts* **2022**, *12*, 983. [[CrossRef](#)]
15. Khan, S.; Han, C.; Sayed, M.; Sohail, M.; Jan, S.; Sultana, S.; Khan, H.M.; Dionysiou, D.D. Exhaustive photocatalytic lindane degradation by combined simulated solar light-activated nanocrystalline TiO₂ and inorganic oxidants. *Catalysts* **2019**, *9*, 425. [[CrossRef](#)]
16. Sultana, S.; Hayata, A.; Sayed, M.; Rehanc, I.; Rehand, K.; Tabassumb, S.; Amine, N.U.; Khanf, S.; Khane, A.; Shahb, L.A. Photo-fenton oxidation of dichlorophene in aqueous solution: Kinetics investigation and effects of operational parameters. *Desalination Water Treat.* **2021**, *222*, 295–301. [[CrossRef](#)]
17. Khan, S.; Sayed, M.; Sohail, M.; Shah, L.A.; Raja, M.A. Advanced oxidation and reduction processes. In *Advances in Water Purification Techniques*; Elsevier: Amsterdam, The Netherlands, 2019; pp. 135–164.

18. Khan, J.A.; Sayed, M.; Khan, S.; Shah, N.S.; Dionysiou, D.D.; Boczkaj, G. Advanced oxidation processes for the treatment of contaminants of emerging concern. In *Contaminants of Emerging Concern in Water and Wastewater*; Elsevier: Amsterdam, The Netherlands, 2020; pp. 299–365.
19. Malika, M.; Sonawane, S.S. The sono-photocatalytic performance of a Fe₂O₃ coated TiO₂ based hybrid nanofluid under visible light via rsm. *Colloids Surf. A Physicochem. Eng. Asp.* **2022**, *641*, 128545. [[CrossRef](#)]
20. Fouda, A.; Hassan, S.E.-D.; Saied, E.; Azab, M.S. An eco-friendly approach to textile and tannery wastewater treatment using maghemite nanoparticles (γ -Fe₂O₃-NPs) fabricated by *Penicillium expansum* strain (Kw). *J. Environ. Chem. Eng.* **2021**, *9*, 104693. [[CrossRef](#)]
21. Fouda, A.; Eid, A.M.; Abdelkareem, A.; Said, H.A.; El-Belely, E.F.; Alkhalifah, D.H.M.; Alshallash, K.S.; Hassan, S.E.-D. Phyco-synthesized zinc oxide nanoparticles using marine macroalgae, *Ulva fasciata delile*, characterization, antibacterial activity, photocatalysis, and tanning wastewater treatment. *Catalysts* **2022**, *12*, 756. [[CrossRef](#)]
22. Mallikarjuna, K.; Vattikuti, S.V.P.; Manne, R.; Manjula, G.; Munirathnam, K.; Mallapur, S.; Marraiki, N.; Mohammed, A.; Reddy, L.V.; Rajesh, M. Sono-chemical synthesis of silver quantum dots immobilized on exfoliated graphitic carbon nitride nanostructures using ginseng extract for photocatalytic hydrogen evolution, dye degradation, and antimicrobial studies. *Nanomaterials* **2021**, *11*, 2918. [[CrossRef](#)]
23. Khitab, F.; Jan, M.R.; Shah, J. Removal of hazardous textile dyes from water using Ni impregnated ZnO through sonophotocatalytic degradation. *Desalination Water Treat.* **2020**, *205*, 357–372. [[CrossRef](#)]
24. Zuorro, A.; Lavecchia, R.; Monaco, M.M.; Iervolino, G.; Vaiano, V. Photocatalytic Degradation of Azo Dye Reactive Violet 5 on Fe-Doped Titania Catalysts under Visible Light Irradiation. *Catalysts* **2019**, *9*, 645. [[CrossRef](#)]
25. Shah, J.; Jan, M.R.; Khitab, F. Sonophotocatalytic degradation of textile dyes over Cu impregnated ZnO catalyst in aqueous solution. *Process Saf. Environ. Prot.* **2018**, *116*, 149–158. [[CrossRef](#)]
26. Mousavi, S.M.; Mahjoub, A.R.; Abazari, R. Facile green fabrication of nanostructural Ni-doped ZnO hollow sphere as an advanced photocatalytic material for dye degradation. *J. Mol. Liq.* **2017**, *242*, 512–519. [[CrossRef](#)]
27. Gholami, M.; Shirzad-Siboni, M.; Yang, J.-K. Application of Ni-doped ZnO rods for the degradation of an azo dye from aqueous solutions. *Korean J. Chem. Eng.* **2016**, *33*, 812–822. [[CrossRef](#)]
28. Irfan, M.; Zahid, M.; Tahir, N.; Yaseen, M.; Qazi, U.; Javaid, R.; Shahid, I. Enhanced photo-Fenton degradation of Rhodamine B using iodine-doped iron tungstate nanocomposite under sunlight. *Int. J. Environ. Sci. Technol.* **2022**, *20*, 3645–3660. [[CrossRef](#)]
29. Khan, S.; Han, C.; Khan, H.M.; Boccelli, D.L.; Nadagouda, M.N.; Dionysiou, D.D. Efficient degradation of lindane by visible and simulated solar light-assisted S-TiO₂/peroxymonosulfate process: Kinetics and mechanistic investigations. *Mol. Catal.* **2017**, *428*, 9–16. [[CrossRef](#)]
30. Sherin, J.J.; Bessy, T.; Asha, S.; Kumar, C.V.; Huessien, D.; Bindhu, M.; Rasheed, R.A.; Alarjani, K.M. Microwave assisted hydrothermally synthesized cobalt doped zinc ferrites nanoparticles for the degradation of organic dyes and antimicrobial applications. *Environ. Res.* **2022**, *208*, 112687. [[CrossRef](#)]
31. Neralekere Somashekar, A.K.; Malingappa, P. Solvothermal synthesis of reduced graphene oxide and zinc ferrite containing composite and its application as an electrochemical sensor in simultaneous measurement of lead, cadmium and mercury ions. *J. Iran. Chem. Soc.* **2022**, *19*, 3481–3490. [[CrossRef](#)]
32. Riaz, A.; Khan, M.A.; Junaid, M.; Gulbadan, S.; Manzoor, A.; Ejaz, S.R.; Ashraf, G.A.; Smaili, H.; Morsi, M.; Alshahrani, T. Effect of Nd³⁺ ions on structural, spectral, magnetic, and dielectric properties of Co–Zn soft ferrites synthesized via sol-gel technique. *Mater. Chem. Phys.* **2022**, *290*, 126519. [[CrossRef](#)]
33. Zakaly, H.M.; Issa, S.A.; Saudi, H.; Alharshan, G.A.; Uosif, M.; Henaish, A. Structure, mössbauer, electrical, and γ -ray attenuation-properties of magnesium zinc ferrite synthesized co-precipitation method. *Sci. Rep.* **2022**, *12*, 15495. [[CrossRef](#)]
34. Xu, S.; Liu, D.; Liu, A.; Sun, F.; Pan, S.; Ouyang, H. Adsorption performances and electrochemical characteristics of methyl blue onto magnesium-zinc ferrites. *Mater. Res. Express* **2022**, *9*, 015002. [[CrossRef](#)]
35. Aziz, N.; Rasool, S.; Ullah, T.; Khitab, F.; Halim, S.A.; Bawazeer, S.; Khan, A.; Al-Harrasi, A. Sonophotocatalytic Degradation of Fast Yellow AB and Remazol Brilliant Violet-5R by Using Ag-Impregnated ZnO as a Photocatalyst. *ACS Omega* **2023**, *8*, 18509–18515. [[CrossRef](#)] [[PubMed](#)]
36. Ullah, T.; Gul, H.; Khitab, F.; Khattak, R.; Ali, Y.; Rasool, S.; Khan, M.S.; Zekker, I. Adsorption of remazol brilliant violet-5r from aqueous solution using sugarcane bagasse as biosorbent: Kinetic and thermodynamic studies. *Water* **2022**, *14*, 3014. [[CrossRef](#)]
37. Mansour, S.; Wageh, S.; Al-Wafi, R.; Abdo, M. Enhanced magnetic, dielectric properties and photocatalytic activity of doped Mg–Zn ferrite nanoparticles by virtue of Sm³⁺ role. *J. Alloys Compd.* **2021**, *856*, 157437. [[CrossRef](#)]
38. Makofane, A.; Motaung, D.E.; Hintsho-Mbita, N.C. Photocatalytic degradation of methylene blue and sulfisoxazole from water using biosynthesized zinc ferrite nanoparticles. *Ceram. Int.* **2021**, *47*, 22615–22626. [[CrossRef](#)]
39. Shakil, M.; Inayat, U.; Khalid, N.; Tanveer, M.; Gillani, S.; Tariq, N.; Shah, A.; Mahmood, A.; Dahshan, A. Enhanced structural, optical, and photocatalytic activities of Cd–Co doped Zn ferrites for degrading methyl orange dye under irradiation by visible light. *J. Phys. Chem. Solids* **2022**, *161*, 110419. [[CrossRef](#)]
40. Oliveira, T.P.; Marques, G.N.; Castro, M.A.M.; Costa, R.C.V.; Rangel, J.H.G.; Rodrigues, S.F.; dos Santos, C.C.; Oliveira, M.M. Synthesis and photocatalytic investigation of ZnFe₂O₄ in the degradation of organic dyes under visible light. *J. Mater. Res. Technol.* **2020**, *9*, 15001–15015. [[CrossRef](#)]

41. Rameshbabu, R.; Ramesh, R.; Kanagesan, S.; Karthigeyan, A.; Ponnusamy, S. Synthesis and study of structural, morphological and magnetic properties of ZnFe₂O₄ nanoparticles. *J. Supercond. Nov. Magn.* **2014**, *27*, 1499–1502. [[CrossRef](#)]
42. Iqra; Khattak, R.; Begum, B.; Qazi, R.A.; Gul, H.; Khan, M.S.; Khan, S.; Bibi, N.; Han, C.; Rahman, N.U. Green Synthesis of Silver Oxide Microparticles Using Green Tea Leaves Extract For An Efficient Removal of Malachite Green From Water: Synergistic Effect of Persulfate. *Catalysts* **2023**, *13*, 227. [[CrossRef](#)]
43. Jaafar, N.F.; Jalil, A.A.; Triwahyono, S.; Ripin, A.; Ali, M.W. Significant effect of pH on photocatalytic degradation of organic pollutants using semiconductor catalysts. *J. Teknol.* **2016**, *78*, 7–12. [[CrossRef](#)]
44. Singh, V.; Singh, J.; Srivastava, P. Synthesis and Characterization of Acacia Gum-Fe⁰Np-Silica Nanocomposite: An Efficient Fenton-Like Catalyst for the Degradation of Remazol Brilliant Violet Dye. *Appl. Nanosci.* **2018**, *8*, 793–810. [[CrossRef](#)]
45. Rápó, E.; Posta, K.; Suciú, M.; Szép, R.; Tonk, S. Adsorptive Removal of Remazol Brilliant Violet-5R Dye from Aqueous Solutions Using Calcined Eggshell as Biosorbent. *Acta Chim. Slov.* **2019**, *66*, 648–658. [[CrossRef](#)] [[PubMed](#)]
46. Reza, K.M.; Kurny, A.; Gulshan, F. Parameters affecting the photocatalytic degradation of dyes using TiO₂: A review. *Appl. Water Sci.* **2017**, *7*, 1569–1578. [[CrossRef](#)]
47. Ensing, B.; Buda, F.; Baerends, E.J. Fenton-like chemistry in water: Oxidation catalysis by Fe(III) and H₂O₂. *J. Phys. Chem. A* **2003**, *107*, 5722–5731. [[CrossRef](#)]
48. Aly, H.F.; Abd-Elhamid, A.I. Photocatalytic Degradation of Methylene Blue Dye Using Silica Oxide Nanoparticles as a Catalyst. *Water Environ. Res.* **2018**, *90*, 807–817. [[CrossRef](#)]
49. Wang, X.-Q.; Han, S.-F.; Zhang, Q.-W.; Zhang, N.; Zhao, D.-D. Photocatalytic Oxidation Degradation Mechanism Study of Methylene Blue Dye Waste Water with GR/iTO₂. *MATEC Web Conf.* **2018**, *238*, 03006. [[CrossRef](#)]
50. Zainip, V.J.; Adnan, L.A.; Elshikh, M.S. Decolorization of Remazol Brilliant Violet 5R and Procion red MX-5B by Trichoderma Species. *Trop. Aquat. Soil Pollut.* **2021**, *1*, 108–117. [[CrossRef](#)]
51. Bheemaraddi, M.C.; Patil, S.; Shivannavar, C.T.; Gaddad, S.M. Isolation and characterization of *Paracoccus* sp. GSM₂ capable of degrading textile azo dye Reactive Violet 5. *Sci. World J.* **2014**, *2014*, 410704. [[CrossRef](#)]
52. Cabansag, J.L.J.; Dumelod, J.C.; Alfaro, J.C.O.; Arsenal, J.D.; Sambot, J.C.; Enerva, L.T.; Leño, J.L., Jr. Photocatalytic Degradation of Aqueous C.I. Reactive Violet 5 Using Bulk Zinc Oxide (ZnO) Slurry. *Philipp. J. Sci.* **2013**, *142*, 77–85.
53. Abbasian, A.R.; Shafiee Afarani, M. One-step solution combustion synthesis and characterization of ZnFe₂O₄ and ZnFe_{1.6}O₄ nanoparticles. *Appl. Phys. A* **2019**, *125*, 721. [[CrossRef](#)]

Disclaimer/Publisher's Note: The statements, opinions and data contained in all publications are solely those of the individual author(s) and contributor(s) and not of MDPI and/or the editor(s). MDPI and/or the editor(s) disclaim responsibility for any injury to people or property resulting from any ideas, methods, instructions or products referred to in the content.